



1 Identification and characterization of foehn events in 2 Beijing and their impact on air-pollution episodes

3 Ju Li^{1,2,3}, Jingjiang Zhang^{1,2}, Mengxin Bai⁴, Jie Su^{1,2}, Qingchun Li^{1,2}, Xingcan Jia^{1,2}

4

5 ¹Institute of Urban Meteorology, Beijing, China

6 ²Beijing Research Center for Urban Meteorological Engineering and Technology, Beijing, China

7 ³State Key Laboratory of Severe Weather, Chinese Academy of Meteorological Sciences, Beijing,
8 China

9 ⁴Beijing Municipal Climate Center, Beijing, China

10 Correspondence to: Ju Li (jli@ium.cn)

11 **Abstract.** This study proposes a method for identifying foehn events in Beijing using automatic weather
12 station (AWS) data, considering upper-air wind direction, topography, meteorological changes, and
13 foehn propagation. Analysis of AWS data from 2015 to 2020 revealed an annual average of 56.5 foehn
14 days, with these days occurring most frequently in winter and least frequently in summer. High-
15 frequency foehn areas exhibit a band-like distribution from the northwestern mountainous region to the
16 southeastern plains, while low-frequency areas are primarily concentrated in the northeastern plains. The
17 horizontal extent of the foehn influence is maximal in spring and minimal in summer. Foehn-induced
18 hourly temperature increases can exceed 11 °C, peaking from night to early morning. Approximately 67%
19 of pollution episodes are accompanied by foehn events, with foehn duration negatively correlated
20 to pollution episode duration. 60.4% of foehn events coincide with decreasing concentrations of
21 particulate matter of 2.5 µm diameter (PM_{2.5}), while 39.6% show increases. Rapid PM_{2.5}
22 concentration increases (> 50 µg m⁻³/h) primarily correspond to weak foehn events (temperature
23 increase < 2 °C). Foehn winds influence pollution through direct and indirect effects. The direct effect,
24 associated with strong northwesterly pressure gradients, can rapidly decrease pollutant concentrations.
25 The indirect effect, linked to weak pressure gradients, alters the boundary-layer structure, causing slight
26 decreases followed by rapid increases in pollutant concentrations. This foehn identification method,
27 applicable to long-term historical surface observations, facilitates in-depth exploration of the
28 relationships between foehn events and high-impact weather phenomena.



29 **1 Introduction**

30 Foehn winds are local dry, warm winds occurring on the leeward side of mountains, resulting from
31 descending air flows. They are characterized by warm and dry air, often accompanied by strong gusts
32 and a significant reduction in cloud cover on the leeward side of mountain ranges (Brinkmann, 1971;
33 Richner and Hächler, 2013). The term “foehn” originally referred to a warm, dry wind formed in German,
34 Austrian, and Swiss valleys after air flows crossed the Alps (Whiteman, 2000). Other regional foehn-
35 type winds include the Chinook winds on the eastern side of the Rocky Mountains in the United States
36 (Brinkmann, 1974; Durran, 1986) and the Santa Ana winds in Southern California (Raphael, 2003;
37 Guzman-Morales et al., 2016; Rolinski et al., 2019). Foehn winds occur on the leeward slopes of most
38 major mountain ranges worldwide and have been extensively studied. Examples include foehn winds in
39 the Alps (Hoinka, 1985a,b; Gohm and Mayr, 2004; Jaubert et al., 2005; Drobinski et al., 2007; Cetti and
40 Sprenger, 2015; Haid et al., 2020), Japan (Kusaka and Fudeyasu, 2017), New Zealand (McGowan and
41 Sturman, 1996; McGowan et al., 2002), and the Antarctic Peninsula (Orr et al., 2008; Elvidge et al., 2016;
42 Turton et al., 2018; Elvidge et al., 2020). These dry, warm winds impact agriculture, ecosystems, and
43 climate systems, affecting plant growth and development (Walker and Ruffner, 1998) and increasing the
44 risk of avalanches, floods, and glacier melting (Barry 2008; Cook et al. 2005; Kuipers Munneke et al.,
45 2012). Strong gusts associated with foehn winds can damage buildings and property, potentially
46 triggering and rapidly spreading wildfires (Westerling et al. 2004; Sharples et al. 2010). Foehn winds can
47 also exacerbate the effects of heatwaves (Takane and Kusaka, 2011; Nishi and Kusaka, 2019; Nishi et
48 al., 2019; Lian et al., 2008) and influence air-pollution levels by affecting pollutant transport and altering
49 the boundary-layer structure (Li et al., 2015; Li et al., 2020).

50 The formation of foehn winds is commonly attributed to terrain-induced latent heat release and
51 precipitation mechanisms, which are widely adopted in textbooks. Currently, four main mechanisms are
52 recognized in the academic community (Seibert et al., 1990; Ólafsson, 2005; Elvidge and Renfrew, 2016):
53 isentropic drawdown, latent heat release and precipitation, mechanical mixing, and radiative heating.
54 Miltenberger et al. (2016) found that thermodynamic effects dominate foehn formation in Switzerland,
55 while Seibert (1990) and Würsch and Sprenger (2015) showed that dynamic effects contribute more
56 significantly. Kusaka et al. (2021) reported that 80.8% of foehn events in Japan occurred without
57 precipitation, suggesting that thermodynamic effects are not always dominant. Foehn formation depends
58 on various factors, including local geography, topography, and weather conditions, and can result from
59 single or multiple mechanisms. Therefore, when studying foehn causes, it is necessary to conduct detailed
60 and comprehensive analyses considering the specific geographical and weather conditions of the research
61 area. Foehn identification methods vary depending on the region and research objectives. A simple
62 approach is to classify days with high temperatures, low humidity, and winds from mountainous areas
63 as foehn days (Shibata et al., 2010); however, this method may misidentify large-scale phenomena as
64 foehn events. Most methods require hourly temperature increases of at least 1 °C, specific surface wind
65 directions, and decreased humidity. Some methods also include wind speed thresholds and quantitative
66 humidity reduction requirements (Speirs, 2012), while others consider both surface and upper-air wind
67 direction and speed (Kusaka et al., 2021). In addition to surface meteorological observations, many
68 studies utilize reanalysis data and radar observations for foehn identification and trajectory tracking
69 (Kusaka et al., 2021; Jansing et al., 2022).

70 The eastern foothills of the Taihang Mountains are prone to foehn winds, which have extensive
71 impacts on the North China Plain’s agricultural production, heatwaves, and air pollution. Consequently,



72 Taihang Mountain foehn events have attracted significant research attention and are one of the hotspots
73 in Chinese foehn research (Zhao et al., 1993; Xiong et al., 2020; Wang et al., 2012a, 2012b). Various
74 identification methods have been developed for Taihang Mountain foehn, such as those proposed by
75 Zhao et al. (1993), Wang et al. (2012a), and Xiong et al. (2020). However, these studies primarily focus
76 on the central and southern sections of the Taihang Mountains. Beijing's main urban area and population
77 are concentrated in the plain formed by the intersection of the northern Taihang Mountains and the
78 Yanshan Mountains (also known as the "Beijing Bay"), which is susceptible to Taihang Mountain foehn
79 winds. Due to the distinct environmental differences between Beijing and the central and southern
80 Taihang Mountains, existing foehn identification methods and derived climatic characteristics may not
81 accurately represent the foehn winds affecting Beijing. Therefore, it is necessary to develop a foehn
82 identification method specifically tailored to Beijing's unique geographical environment and weather
83 conditions, and to conduct long-term foehn characteristic analysis based on this method.

84 Foehn winds can influence the transport and distribution of atmospheric pollutants. For example, the
85 collision of foehn winds with valley winds in canyon topography can lead to severe air-pollution events
86 (Li et al., 2015), and foehn winds can cause horizontal and vertical transport of ozone (Seibert et al.,
87 2000). The North China Plain, east of the Taihang Mountains, is one of China's most severely air-
88 polluted regions. The area's severe air pollution problems are related to high local pollution emissions
89 (Zhao et al., 2012) and complex terrain, land use, and land cover that induce local circulations such as
90 mountain-valley winds, sea-land breezes, and urban heat-island circulations (Liu et al., 2009; Wang et
91 al., 2017). These factors influence pollutant transport and lead to severe air-pollution events (Zheng et
92 al., 2015; Sun et al., 2016; Ma et al., 2017). Despite this, there have been few studies on the impact of
93 foehn events on air pollution in this region. Yang et al. (2008) analyzed the effects of Taihang Mountain
94 foehn winds on PM_{2.5} concentrations, finding that foehn winds can reduce PM_{2.5} concentrations and
95 increase visibility in plain areas. Li et al. (2020) proposed that foehn winds can indirectly exacerbate air
96 pollution based on an analysis of a pollution process with a haze front and discovered a close connection
97 between foehn events and pollution events. However, due to the lack of analysis of more pollution events,
98 there is insufficient understanding of the relationship between foehn winds and pollution events. It is
99 necessary to utilize observational data from a wider range and longer time series to study the relationship
100 between foehn winds and pollution events, further revealing the impact and mechanisms of foehn winds
101 on air pollution.

102 The objective of this paper is to establish a foehn identification method for the Beijing area based on
103 AWS data, conduct foehn characteristic analysis, and investigate the relationship between foehn winds
104 and pollution events. The article is divided into seven chapters. Following the introduction, Chapter 2
105 introduces the data and methods used, Chapter 3 focuses on foehn identification, and Chapter 4 presents
106 statistical analysis of foehn characteristics. The relationship between pollution events and foehn winds
107 is explored in Chapter 5. Chapter 6 provides a discussion, and conclusions are presented in Chapter 7.

108 **2 Data and methods**

109 **2.1 Data**

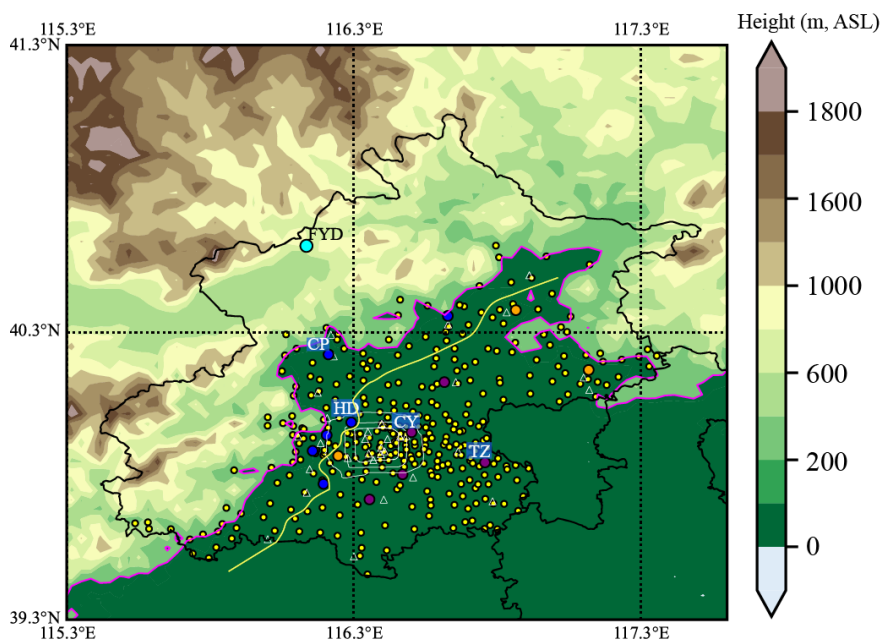
110 Meteorological data used in this study comprise hourly observations from all operational Automatic
111 Weather Stations (AWSs) in the Beijing area from 2015 to 2020. The observed elements include
112 temperature, relative humidity, pressure, precipitation, and 2-minute average wind direction and speed.



113 AWSs were categorized into Plain AWSs (PAWSs, elevation ≤ 200 meters) and mountain AWSs (Non-
114 PAWSs, elevation > 200 meters). Among the mountain stations, Foyeding Station (FYD, elevation
115 1224.9 meters) was selected as the representative High-Mountain AWS (HMAWS). Located on a
116 mountaintop at the northwestern border of Beijing and Hebei Province, its wind measurements are
117 approximately representative of upper-air winds at around 900 hPa. Figure 1 illustrates the distribution
118 of AWSs used in this study. Among the plain stations, 14 are national stations, while the rest are regional
119 stations. National stations are installed in standard meteorological fields, compliant with WMO
120 observation regulations, providing better observational environments and higher data quality, as well as
121 more continuous data compared to regional stations. All national stations have observational data for the
122 selected 6-year period, while some regional stations lack data for earlier years, as they were not yet
123 established. Based on their proximity to mountainous areas, plain national stations were further classified
124 into Near-Mountain Plain AWSs (NM-PNAWS, large blue dots in Fig. 1, totaling six stations) and Non-
125 Near-Mountain Plain AWSs (large orange and purple dots in Fig. 1).

126 Air-pollution data consist of hourly PM_{2.5} concentration values from 33 environmental monitoring
127 stations (white triangles in Fig. 1) within Beijing, published by the Ministry of Ecology and Environment.
128 The data cover the same time range as the meteorological data and can be downloaded from
129 <https://quotsoft.net/air/>. The hourly average PM_{2.5} concentration across the 33 environmental
130 monitoring stations was calculated to obtain a city-wide average PM_{2.5} concentration time series.
131 Continuous periods with city-wide average PM_{2.5} concentrations exceeding $35 \mu\text{g m}^{-3}$ and a mean value
132 greater than $75 \mu\text{g m}^{-3}$ were defined as pollution episodes. The pollutant concentration changes
133 associated with foehn winds were categorized into two types: rapid pollutant concentration
134 decrease (Type I) and slight pollutant concentration decrease followed by a rapid increase (Type II).

135 Sea-level-pressure (SLP) data from the European Centre for Medium-Range Weather Forecasts
136 (ECMWF) ERA reanalysis were used to determine weather patterns associated with different foehn types
137 during pollution episodes. Data with a horizontal resolution of $0.25^\circ \times 0.25^\circ$ covering latitudes 32°N to
138 51°N and longitudes 100°E to 130°E were utilized, and Self-Organizing Maps (SOMs) were employed
139 for weather pattern classification.



140

141 **Figure 1: Distribution of observation sites in Beijing, China.** The map shows the locations of various
142 Automatic Weather Stations (AWSs): small yellow dots represent Regional AWSs situated at elevations below
143 200 meters. The large light-blue dot indicates the High-Mountain Station at FYD. Large dark-blue dots
144 represent the Near-Mountain Plain National AWSs (NM-PNAWS). Large purple dots denote the National
145 AWSs in the central and eastern plain areas. Large orange dots mark other National AWSs in the plain area.
146 Some key National AWSs are labeled with their name abbreviations. White triangles represent air-pollution
147 monitoring stations. The white concentric circles respectively represent the Third, Fourth, and Fifth Ring
148 Roads. The pink lines indicate the contour line at an elevation of 200 m. The AWSs located between the pink
149 and yellow lines are stations selected as the Near-Mountain Plain AWSs (NM-PAWS).

150

151 2.2 Methods

152 For weather pattern classification associated with different foehn types during pollution episodes, we
153 applied the SOM method (Kohonen, 1995). SOM has been widely applied in meteorological research
154 (Rolinski et al., 2019; Ohba and Sugimoto, 2020; Liao et al., 2020) and in classifying weather patterns
155 associated with foehn winds (Kusaka et al., 2021). This method comprises a neural network that uses
156 unsupervised learning to produce low-dimensional representations of high-dimensional input vectors.
157 SOMs consist of input and output (competitive) layers, mapping high-dimensional samples from the
158 input layer to one- or two-dimensional grids in the output layer. The number of output layer nodes equals
159 the number of clusters (N). For different pollution stages (on a daily basis), SLP data from NCEP were
160 used to train the SOM model. We used 9317 SLP grid points, with the SLP spatial field for each pollution
161 day serving as a vector field. The input layer was set to m samples (80 and 33 for the Type I and Type II



162 foehn winds during pollution episodes, respectively). The input pattern can be denoted as $X = \{x_i; i =$
163 $1, \dots, m\}$; the output layer contains n neurons, denoted as $Y = \{y_j; j = 1, \dots, n\}$; and the connection weight
164 between input unit i and output layer neuron j in the computational layer can be written as $W_j = \{w_{ji}; j =$
165 $1, \dots, n; i = 1, \dots, m\}$. The mapping relationship between the two is given by equation (1):

$$166$$
$$167 \quad Y = XW, \quad (1)$$
$$168$$

169 During sample training, only one of the n output neurons is optimal, with its weight given by equation
170 (2):

$$171$$
$$172 \quad \Delta w_{ji} = \eta \cdot (x_i - w_{ji}) Y_j. \quad (2)$$
$$173$$

174 where η is the number of training iterations, set to 10,000 in this study. Through weight optimization,
175 the weight vector of the optimal neuron is moved towards the selected input sample. This training
176 iteration process is repeated until convergence, ultimately achieving the learning objective. After
177 multiple tests, the numbers of nodes connecting the input and output layers (i.e., the number of patterns)
178 for the Type I and Type II foehn winds were adjusted to 6 and 4, respectively, yielding the best
179 classification results.

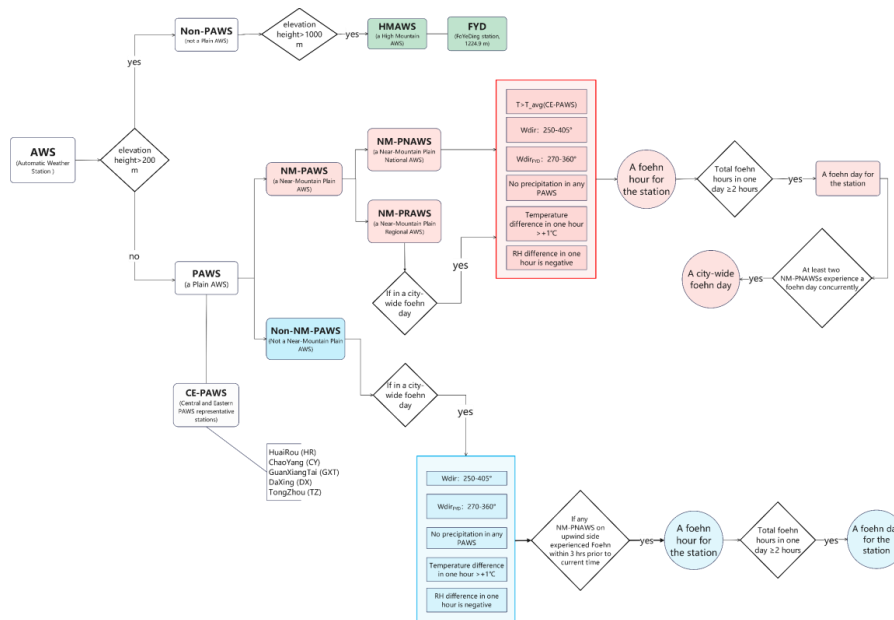
180 **3. Identification of foehn events**

181 Our objective is to develop a method for identifying foehn events based entirely on AWS data. The
182 advantage of this method is that it allows for the identification of foehn events using the same type of
183 observational data over longer time series, facilitating long-term climatic analysis and research of foehn
184 winds. According to the characteristics of foehn winds in the Taihang Mountains (Wang et al., 2012a),
185 the formation of foehn winds in this region requires a background wind from the northwest at high
186 altitudes, with the wind direction roughly perpendicular to the southwest–northeast orientation of the
187 Taihang Mountains. Additionally, the occurrence of a foehn event follows a specific temporal sequence:
188 it first appears in the plain areas near the leeward slope and then sequentially at downstream locations
189 along the foehn propagation path. Therefore, the National Meteorological Station FYD, at an elevation
190 of 1224.9 meters, was selected as the high-altitude wind observation station. This choice avoids issues
191 such as shorter observation periods and data format inconsistencies that can arise from using other high-
192 altitude wind observation data, such as wind profiler radar.

193 By studying 22 representative historical foehn cases, we developed a method for identifying foehn
194 events in the Beijing area based on AWS data (Fig. 2). First, we determine whether a specific station
195 within NM-PNAWS is experiencing a foehn event. If the following conditions are met simultaneously
196 at a given time, then this time is considered a foehn hour at this NM-PNAWS: the wind direction at FYD
197 is northwest ($270\text{--}360^\circ$), there is no precipitation at any plain station, the temperature at this NM-
198 PNAWS exceeds the mean temperature of the representative stations in the Central and Eastern PAWS
199 (CE-PAWSs), the wind direction at NM-PNAWS is $250\text{--}405^\circ$, the hourly temperature change is greater
200 than 1°C , and the hourly relative humidity change is negative. The condition that the temperature at
201 NM-PNAWS must be higher than the average temperature at CE-PAWS is introduced to select the
202 moments at which the temperature rise at this station precedes that at CE-PAWS. If at least two foehn
203 hours occur at the same NM-PNAWS on the same day, that day is defined as a foehn day for that station.



204 If at least two NM-PNAWSs experience foehn days on the same date, that date is defined as a city-wide
 205 foehn day. Identification of a single-station foehn for other plain stations that are not NM-PNAWS is
 206 only conducted on city-wide foehn days. This involves sequentially identifying single-station foehn
 207 hours and station foehn days, as detailed in Fig. 2.



208
 209 **Figure 2: Flowchart of foehn identification based on AWS data.**

210 **4. Analysis of foehn characteristics**

211 Based on the aforementioned methodology, foehn days at all PAWSs in Beijing were identified for the
 212 period from January 1, 2015 to December 31, 2020. The temporal variation of foehn days across all
 213 PAWSs in the Beijing region over six years is summarized (Table 1). The six-year average number of
 214 foehn days for all PAWSs is 56.5, with notable differences in both the annual mean and maximum foehn
 215 days among years, exhibiting an undulating trend over time. The highest average was observed in 2016
 216 with 64.4 days, while the lowest occurred in 2017 with 47.6 days. The maximum number of foehn days
 217 peaked at 118 days in 2020 and bottomed out at 90 days in 2015.

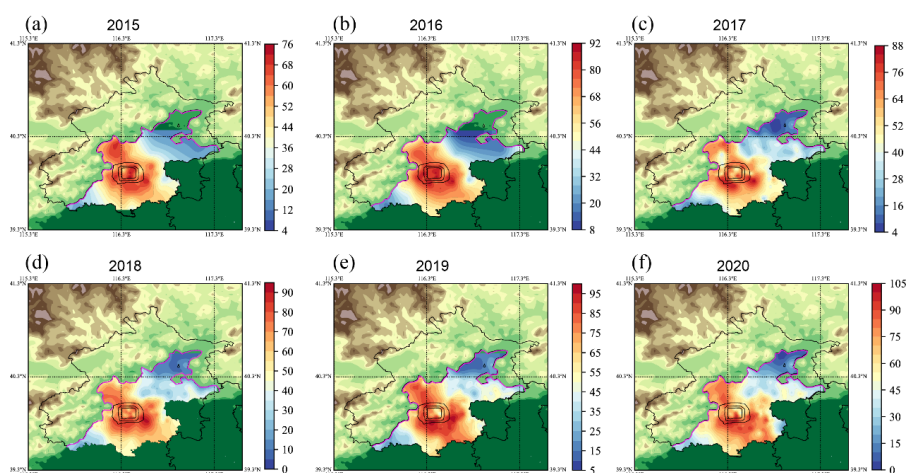
218
 219 **Table 1. Annual statistics of foehn days at Plain AWSs in the Beijing area.**

Year	2015	2016	2017	2018	2019	2020
Annual average number of foehn days	51.7	64.4	47.6	52.9	62.0	59.9
Annual maximum number of foehn days	90.0	105.0	108.0	110.0	115.0	118.0

220
 221 Figure 3 illustrates the annual cumulative distribution of foehn days at PAWSs, revealing a generally



222 consistent horizontal distribution pattern across different years. High-frequency foehn zones are roughly
223 aligned in a northwest-to-southeast direction, indicative of a pronounced impact from the western terrain.
224 Mountain-proximal regions, specifically the western and northwestern parts of Changping District, the
225 western portion of Haidian District, the western section of Mentougou District, Shijingshan District, and
226 parts of the western area of Fangshan District, are characterized as high-frequency foehn occurrence
227 zones. Conversely, areas with fewer foehn days are predominantly found in the northeastern plain of
228 Beijing (in the vicinity of Miyun District). Additionally, some urban areas within the Fifth Ring Road
229 also experience relatively low frequencies of foehn days.

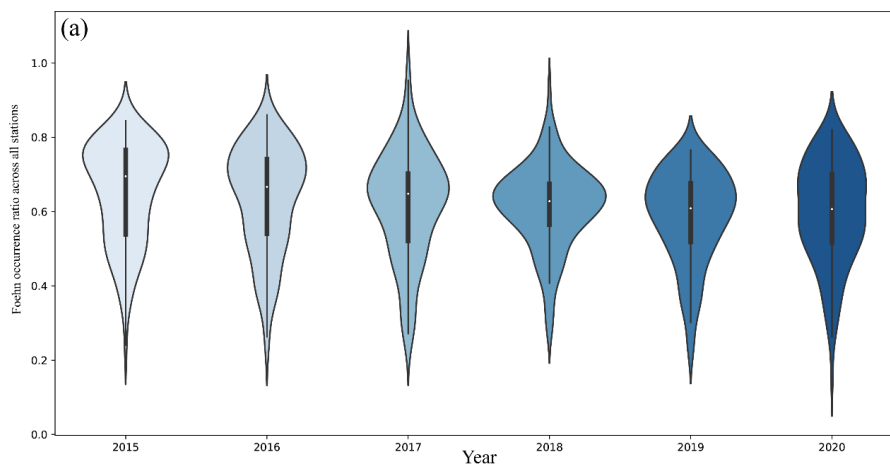


230

231 **Figure 3: Annual distribution of foehn days.**

232

233 To represent the spatial extent of foehn effects, Figure 4 presents violin plots depicting the proportion
234 of stations experiencing foehn winds within the plain areas for each year. More than 50% of the foehn
235 days saw the impact extend over 60% of the stations. There exists inter-annual variability in the
236 horizontal reach of foehn winds. Most years exhibit a unimodal “spindle-shaped” violin plot with a
237 prominent midsection, suggesting a more concentrated distribution of foehn influence within specific
238 ranges. Notably, 2015 and 2016 demonstrated more extensive foehn impacts, with their peak station
239 percentage exceedance surpassing 70%. In 2020, while the distribution maintained a spindle shape, it
240 lacked a distinct peak; the majority of samples fell within the 50% to 70% interval without a clear modal
241 value, marking the lowest median across the six years. Analyzing the yearly medians suggests an overall
242 trend of a narrowing foehn impact scope over time.



243
 244
 245
 246
 247
 248
 249
 250
 251
 252

Figure 4: Violin plot of the annual distribution of foehn day occurrences across all PAWSs.

Table 2 compiles the monthly counts of foehn days for all PAWSs in the Beijing region. The multi-year monthly average peaks in January with 8.6 days and bottoms out in July with 1.1 days. The monthly maximum number of foehn days reaches its apex in January with 16 days and reaches its nadir in July with 2.5 days. Seasonally, winter sees the highest frequency of foehn days, followed by spring and autumn, with summer having the least.

Table 2. Monthly statistics of foehn days at PAWSs in the Beijing area.

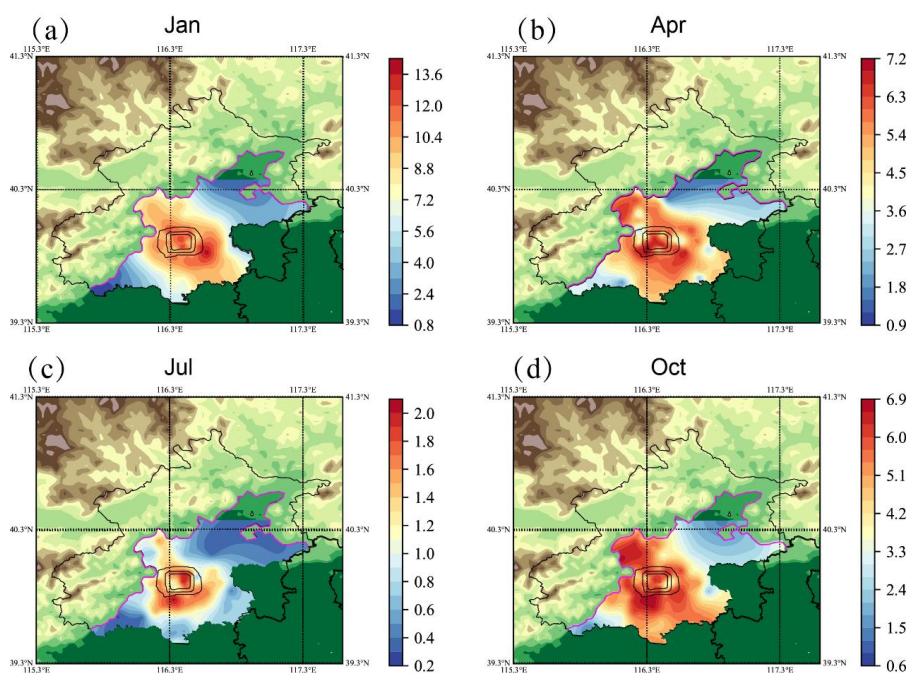
Month	1	2	3	4	5	6	7	8	9	10	11	12
Monthly average number of foehn days	8.6	7.6	6.7	5	5.6	3.2	1.1	3.3	5.1	5	4.3	6.2
Monthly maximum number of foehn days	16	13	12.3	8.3	9.7	5.7	2.5	5.8	9.3	8.7	8.8	11.8

253
 254
 255
 256
 257
 258
 259
 260
 261
 262
 263
 264
 265
 266
 267

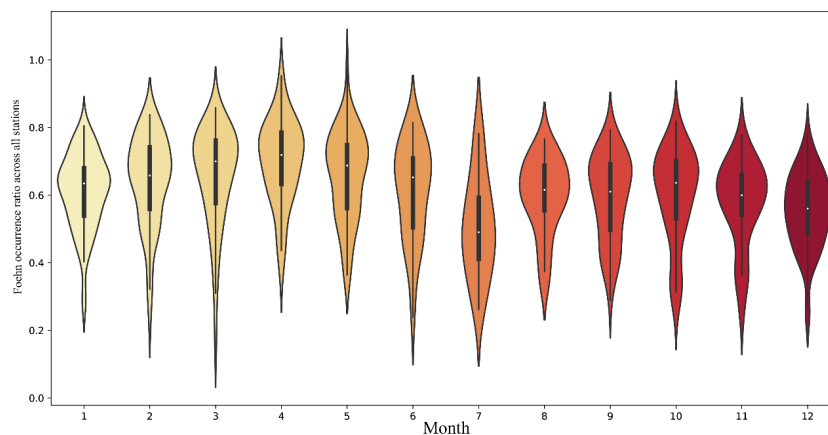
Marked disparities are evident in the seasonal variation of the horizontal distribution of foehn days. While the general pattern of high-value zones for the monthly average foehn days resembles that of the annual total, individual months exhibit differing ranges, leading to discernible discrepancies in their horizontal distribution forms (Fig. 5). January, April, July, and October are selected to represent their four respective seasons. Overall, foehn day frequencies peak in winter, followed by spring and autumn, with summer witnessing the least. In terms of horizontal distribution, winter’s foehn days feature two high-value zones, one in the central urban district and another beyond the southeastern Fifth Ring Road, with the latter recording the highest values. Spring identifies three high-value zones: the mountain-adjacent interface of Changping District and Haidian District, the southwestern part of the central city, and again beyond the southeastern Fifth Ring Road, with the maximum located in the southwestern corner of the central city. Autumn also highlights three high-value zones, mirroring those of spring but with slightly higher values around the Changping–Haidian mountain interface and southwestern Fifth Ring Road outskirts. Summer discerns two high-value zones in the northeastern central city and south of the Fifth Ring Road, with the southern periphery recording the highest. Regarding the monthly variation



268 in the extent of the foehn influence (Fig. 6), April experiences the broadest impact, with July witnessing
269 the narrowest. The seasonal variation in foehn influence generally shows a maximum in spring and a
270 minimum in summer. Except for October and November, violin plots for most months present a unimodal
271 “spindle-type,” indicative of a concentrated distribution. However, October and November uniquely
272 display a bimodal pattern with a secondary, weaker peak in the lower range, suggesting that, while the
273 majority of foehn days in these months affect over 50% of stations, a considerable portion (approximately
274 40%) still experiences a limited foehn impact zone.



275
276 **Figure 5: Multi-year average monthly distribution of foehn days.**
277



278
279 **Figure 6: Violin plot of the monthly distribution of foehn day occurrences across all PAWSs.**

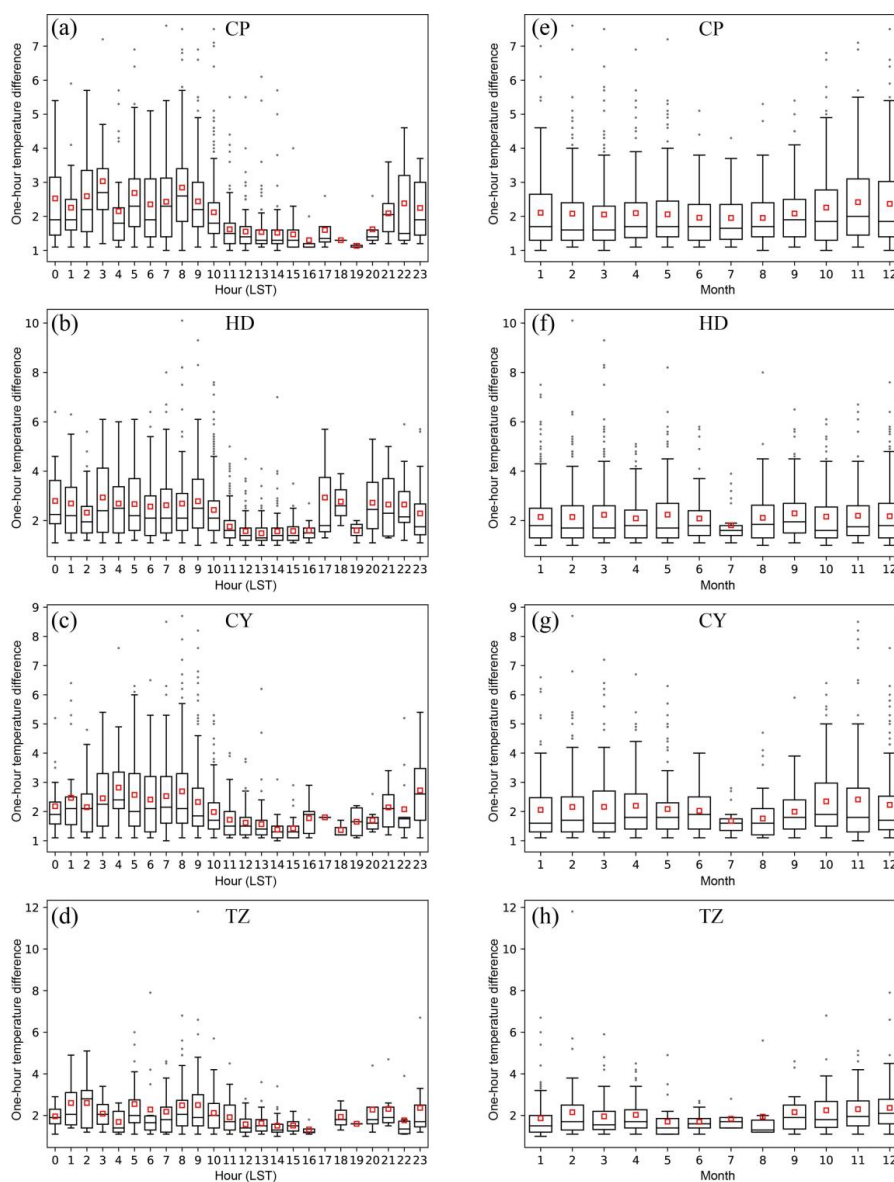


280 To assess the variations in temperature rise induced by foehn winds across different locations, we
281 selected four national meteorological stations—Changping (CP), Haidian (HD), Chaoyang (CY), and
282 Tongzhou (TZ)—situated along a path extending from the leeward side of the northwest mountains
283 toward the southeastern plain (Fig. 1). We analyzed their hourly temperature increments on foehn days.
284 According to Table 3, the median hourly temperature increases at these stations are very similar, ranging
285 from 1.7–1.8 °C. The mean hourly warming fluctuates between 2.0–2.2 °C, with HD experiencing the
286 highest increase and TZ experiencing the least. The maximum hourly warming is greatest at TZ (11.8 °C),
287 followed by HD (10.1 °C), and then CP (7.5 °C). When examining the 25th and 75th percentile values,
288 half of the hourly warming instances at each station fall within a 1.3–2.6 °C range; however, the warming
289 span for TZ is narrower than the other three stations, confined to 1.3–2.4 °C.

290
291 **Table 3.** Statistical values of hourly temperature changes at the selected stations.

	CP	HD	CY	TZ
max	7.5	10.1	8.7	11.8
median	1.7	1.8	1.7	1.7
mean	2.1	2.2	2.1	2
25th Percentile	1.3	1.3	1.3	1.3
75th Percentile	2.6	2.6	2.5	2.4

292
293 In terms of daily variations in hourly temperature changes across these stations (Fig. 7a–d), the periods
294 of minimal warming (troughs) typically occur from midday until before sunset. The trough for CP, which
295 is nearest to the mountains, lasts from 11:00 AM to 8:00 PM, while for HD, CY, and TZ these periods
296 are from 12:00 PM to 5:00 PM, 12:00 PM to 3:00 PM, and 12:00 PM to 5:00 PM, respectively. All
297 stations exhibit two pronounced peaks in their hourly warming patterns each day, occurring around
298 midnight before sunrise and around 8:00 or 9:00 AM post sunrise. There are also typically milder
299 warming peaks around sunset, with HD displaying the most pronounced pre-sunset warming peak among
300 the stations. Observing the monthly changes in hourly warming (Fig. 7e–h), CP, being closest to the
301 mountains, exhibits the broadest range of warming fluctuations, whereas TZ, the farthest from the
302 mountains, shows the narrowest range. The monthly mean warming values are typically lowest in July
303 for all stations, coinciding with the month having the smallest range of warming fluctuations. The average
304 peak warming values are generally seen during autumn (September to November), while the most
305 substantial hourly warming spikes are noted in February.



306

307

308

309

Figure 7: Temporal variations in the hourly temperature changes: (a–d) diurnal variations and (e–h) monthly variations.

310

5. Relationship between pollution episodes and foehn events

311

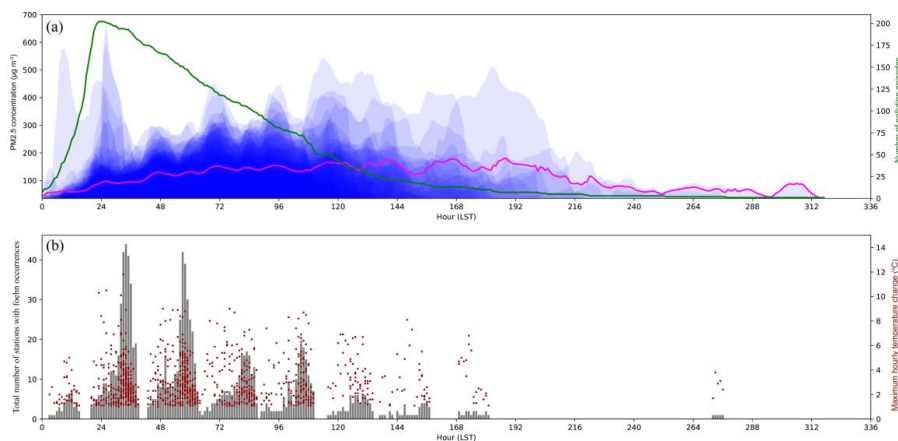
312

313

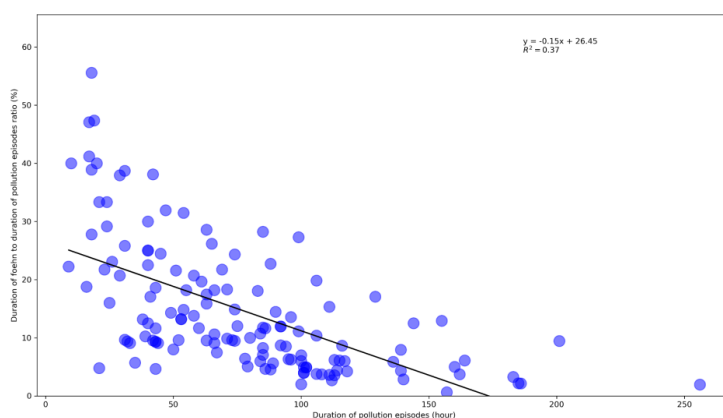
In accordance with the definition of pollution episodes outlined in Chapter 2, 204 qualified pollution episodes during 2015–2020 were identified and visualized in Figure 8. Here, each episode's initiation is marked by its Local Standard Time (LST), with the green line representing the cumulative count of



314 ongoing pollution episodes at each hour and the pink line illustrating the average PM_{2.5} concentration
315 at the respective times. The durations of these pollution episodes mostly remain under 4 days, with
316 instances exceeding 7 days being rare. A conspicuous diurnal pattern in pollutant concentrations is
317 evident, characterized by lower levels during the day and elevated concentrations at night (Fig. 8a).
318 Figure 8b features gray bars that denote the sum of stations experiencing a foehn event at any given time
319 (only considering the 14 plain national stations), reflecting the horizontal reach of the foehn winds. The
320 timing of these peak occurrences aligns with the troughs of pollutant concentrations in Figure 8a,
321 indicating that widespread foehn occurrences coincide with lulls in pollution concentrations. Red scatter
322 points represent the maximum hourly temperature increases during foehn episodes for each time point,
323 and their number for a given moment also signifies the number of pollution episodes experiencing foehn
324 winds at that time. Evidently, foehn winds are more frequent during shorter pollution episodes; as the
325 duration of a pollution episode extends, the likelihood of encountering foehn winds decreases. Generally,
326 the maximum warming magnitude induced by foehn winds tends to decrease as the pollution episode
327 persists longer. Statistics of the 204 pollution episode durations (in hours) reveal a median of 76.6 hours,
328 a mean of 73 hours, a maximum of 313 hours, a minimum of 7 hours, and 25th and 75th percentiles of 42
329 and 101 hours, respectively. The proportion of foehn durations in all pollution episodes is depicted in
330 Figure 9. Among the 204 pollution episodes, 67% (137 episodes) involved foehn occurrences. There is a
331 negative correlation between the proportion of the foehn duration and the length of the pollution episodes,
332 suggesting that longer-lasting pollution episodes see a lower proportion of time affected by foehn winds.
333 On average, foehn winds account for 14.8% of pollution episode durations, reaching a maximum of 55.6%
334 for episodes lasting 18 hours and plummeting to a minimum of 0.6% for episodes enduring 157 hours.



335 **Figure 8: Characteristics of pollution episodes and associated foehn occurrences. (a) Temporal variation of**
336 **the PM_{2.5} concentration during pollution episodes, green line; number of pollution episodes, pink line;**
337 **average PM_{2.5} concentration of pollution episodes. (b) Foehn occurrence during pollution episodes, gray bars;**
338 **cumulative number of stations with foehn occurrences per episode, red scatter points; maximum hourly**
339 **temperature change.**
340

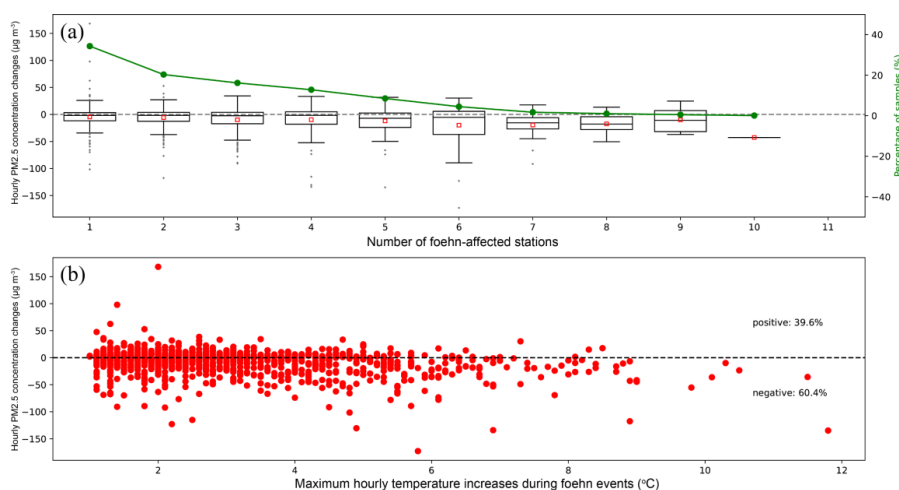


341

342 **Figure 9: Correlation between pollution episode duration and the foehn-to-pollution ratio.**

343

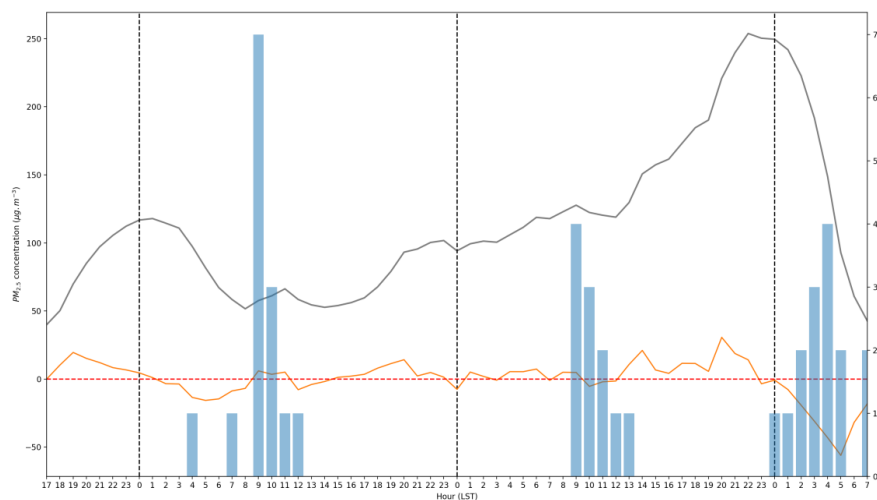
344 Figure 10a illustrates the relationship between hourly variations in PM_{2.5} concentrations and the
345 number of sites experiencing foehn winds. Only the 14 national stations situated in the plain areas are
346 considered for counting the foehn-affected sites. More often than not, foehn events are associated with a
347 decline in the PM_{2.5} concentrations. For processes with a wider foehn influence (more sites reporting
348 foehn winds), the reduction in PM_{2.5} concentrations tends to be more pronounced. Close to 60% of foehn
349 events have an impact range restricted to no more than two stations, with instances of foehn winds
350 affecting over half of the stations being relatively infrequent. Figure 10b relates the hourly changes in
351 PM_{2.5} concentrations to the temperature increase at these sites during foehn events. During foehn periods,
352 60.4% of the time a drop in PM_{2.5} concentrations occurs, while the remainder of the time there is an
353 increase in PM_{2.5} concentrations. The correlation between the maximum temperature rise and changes
354 in the PM_{2.5} concentrations is weakly negative. Pronounced increases in the PM_{2.5} concentrations, such
355 as hourly increments exceeding 50 µg/m³, mainly occur during mild warming phases with temperature
356 increases of less than 2 °C.



357

358 **Figure 10: Relationship between foehn events, PM2.5 concentration changes, and temperature variations.**
359 **(a) Hourly PM2.5 concentration changes in relation to foehn occurrence. Box plot: distribution of hourly**
360 **PM2.5 concentration changes. Green line: percentage of samples in each category. (b) Correlation between**
361 **hourly PM2.5 concentration changes and maximum hourly temperature increases during foehn events.**
362

363 Figure 11 illustrates a typical pollution episode influenced by foehn events, occurring from
364 January 6 to January 9, 2015. Foehn winds were observed during three distinct phases of this episode.
365 Phase I: The foehn initially appeared at isolated stations at 04:00 on January 7, expanding to a
366 widespread occurrence by 09:00. During this phase, pollutant concentrations exhibited a marked
367 decrease, with the widespread foehn event closely following the trough in pollutant concentrations.
368 Phase II: At 09:00 on January 8, a foehn was recorded at four national stations, after which the spatial
369 extent of the foehn influence diminished. During the foehn-affected period, PM2.5 concentrations
370 showed a slight decrease. However, this was followed by a rapid increase in PM2.5 levels, reaching a
371 peak at 22:00. Phase III: Foehn winds reappeared at a single station at 00:00 on January 9, with their
372 influence expanding after 01:00 and reaching maximum extent by 04:00. This phase corresponded to the
373 pollutant clearance stage of the episode, characterized by a rapid decline in PM2.5 concentrations.
374 This case study exemplifies the complex interactions between foehn winds and pollution dynamics,
375 demonstrating both the potential for foehn events to facilitate pollutant dispersion and their role in
376 subsequent rapid accumulation of pollutants under certain conditions.

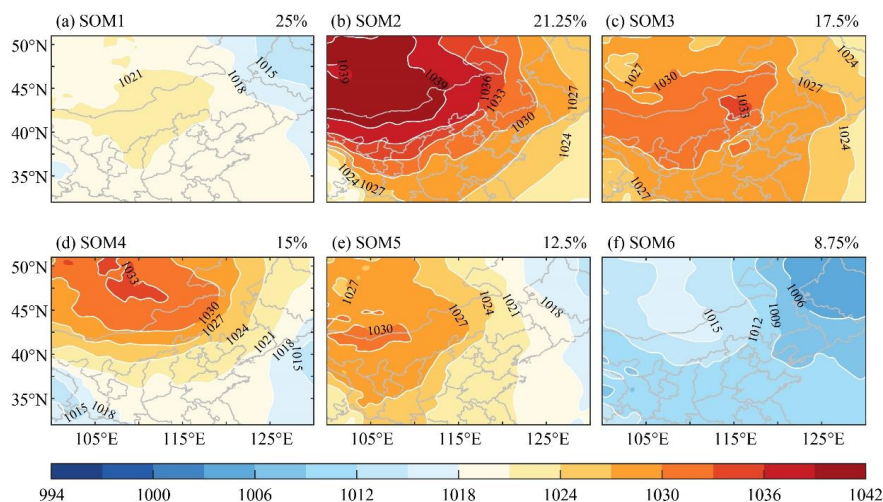


377

378 **Figure 11. Temporal evolution of PM_{2.5} concentrations and foehn event occurrence during a pollution**
379 **episode. Primary Y-axis (left): PM_{2.5} concentration (black line) and hourly PM_{2.5} concentration change**
380 **(orange line). Secondary Y-axis (right): Number of stations experiencing foehn events (blue bars).**

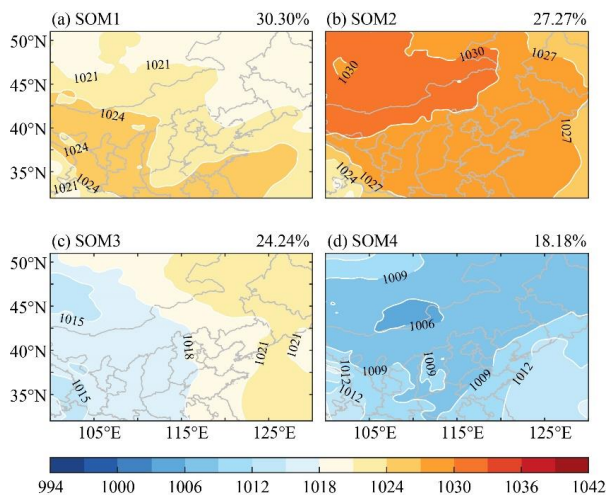
381

382 Through a detailed analysis of additional pollution episodes, we discern two primary categories of
383 pollutant concentration variations associated with foehn events: Type I, characterized by a rapid decline
384 in pollutant concentrations (evident in the first and third phases of Fig. 11), and Type II, which initially
385 exhibits a slight decrease followed by a swift increase in pollutant levels (as observed in the second phase
386 of Fig. 11). We manually classified the 204 pollution episodes involving foehn effects into these two
387 categories, identifying specific dates corresponding to each type, comprising 80 days for Type I and 33
388 days for Type II. Employing the SOM methodology on ERA5 data for these categorized dates, we derived
389 weather typing characteristics that differentiate the impacts of the two foehn types on pollutants. For
390 Type I (depicted in Fig. 12), a consistent high-pressure system is observed northwest of Beijing,
391 accompanied by a pressure gradient directed from northwest to southeast. Notably, SOM types SOM2
392 and SOM4, which feature strong high-pressure systems and pronounced pressure gradients, jointly
393 account for 36.25% of occurrences. These conditions are frequently associated with the passage of cold
394 fronts, facilitating the rapid dispersion of pollutants. SOM3 and SOM5 share similar pressure patterns to
395 SOM2 and SOM4 but exhibit weaker pressure gradients, collectively representing 30% of instances. The
396 SOM1 and SOM6 types display the weakest pressure gradients, together amounting to 33.75% of cases.
397 Regarding Type II, Beijing predominantly resides within a near-isobaric field, with some instances like
398 SOM2 and SOM3 showing weak pressure gradients to the northwest or west of the city. Foehn winds
399 under these types are generally weaker, resulting in only marginal decreases in pollutant concentrations.
400 The subsequent rapid rise in pollutants could be attributed to boundary-layer processes induced by the
401 foehn phenomenon, as suggested by Li et al. (2020).



402
403
404
405

Figure 12: Self-organized classification of the sea-level-pressure patterns associated with Type I foehn events.



406
407
408

Figure 13: Self-organized classification of the sea-level-pressure patterns associated with Type II foehn events.

409 6. Discussion

410 In broader terms, “wind warmed and dried by descent, in general on the lee side of a mountain” can
411 generally be referred to as a foehn wind (WMO, 1992). Identifying the warming and drying effects
412 induced by foehn winds using AWS data presents a challenge in distinguishing such changes from other
413 non-foehn influences, such as heating due to solar radiation or warm air advection not related to foehn
414 events. This issue can be mitigated significantly by incorporating comprehensive analyses of station wind
415 direction and speed fluctuations, along with consistency checks between upstream and downstream wind



416 fields (Zhang and Li, 2024). Consequently, our foehn identification approach begins with stations located
417 in plains adjacent to mountains; only after foehn conditions are detected at these sites do we proceed to
418 identify foehn events at downstream plain stations. For stations near mountainous areas, this
419 methodology effectively pinpoints the onset of foehn occurrences. However, the scenario becomes more
420 intricate for other downstream sites. Factors such as urban influences and diurnal variations in solar
421 radiation can lead to misidentification, where instances of warming not attributable to foehn events might
422 be wrongly classified as such. For example, when the surface wind direction at downstream sites aligns
423 with the foehn wind direction upstream, warming and drying not induced by the foehn may still lead to
424 erroneous identification of a foehn event. Therefore, the results of this study may somewhat overestimate
425 the frequency of foehn wind occurrences at downstream plain stations.

426 Based on the preceding chapter's analysis, it emerges that the impact of foehn winds on pollution
427 events can be primarily categorized into two mechanisms: a reduction in pollutant concentrations and an
428 increase thereof, with the former accounting for over 60% of instances. These mechanisms are
429 respectively referred to as the direct and indirect effects of foehn winds on pollutants (Li et al., 2020).
430 The direct mechanism typically involves a strong pressure gradient perpendicular to the Taihang
431 Mountains, enhancing the intensity of the foehn (manifested by higher wind speeds and temperatures).
432 Northerly foehn winds often carry clean, cold air, leading to a rapid decline in pollutant concentrations
433 and even the termination of pollution episodes. This mechanism commonly operates during the terminal
434 phase of pollution events (the cleanup stage, as seen in Phase III of Fig. 11), though it may also occur in
435 the midst of pollution episodes if the foehn is not potent enough to fully dissipate pollutants (Phase I of
436 Fig. 11). In contrast, the indirect mechanism is more intricate. It corresponds to weather scenarios with
437 an isobaric field or weak pressure gradients. Under such mild meteorological settings, the region in front
438 of the mountains in Jing-Jin-Ji (Beijing-Tianjin-Hebei) is prone to developing local circulations
439 converging towards the mountain front, resulting in the accumulation of pollutants in these areas (Wang
440 and Zhang, 2020). Here, a foehn initially appears on the leeward side, with the formation of a low-
441 pollution, warm, dry air mass advancing southward, encountering a slow-moving, high-pollution, moist,
442 cold air mass from the north, potentially creating a haze front (Li et al., 2020). Given the weak nature of
443 the foehn—characterized by low wind velocities—it fails to induce a rapid decrease or removal of
444 pollutants. A weak pressure gradient force arises between the dissimilar air masses, exacerbated by the
445 waning strength of the foehn over time, causing a seesaw-like exchange that gradually transports
446 pollutants from the south to the cleaner northern regions, thereby elevating pollutant concentrations there.
447 Moreover, the interaction between the warm and cold air masses prompts the warm air to ascend over
448 the cold air, reinforcing the temperature inversion above the cold air mass, which stabilizes the lower
449 atmosphere and exacerbates surface pollution. This indirect mechanism is clearly illustrated during the
450 second phase of the pollution event in Figure 11, where an initial minor decrease in pollutants upon foehn
451 onset is followed by a rapid surge in pollution levels once the foehn subsides.

452 **7. Conclusion**

453 This study utilized data from Beijing's operational AWS network from 2015 to 2020, developing a foehn
454 identification method specifically tailored for the Beijing plain area based entirely on AWS data. The
455 method integrates considerations of the upper-air wind orientation relative to topography, meteorological
456 element variations during foehn passages, and the progressive propagation of foehn winds from leeward



457 slopes to downstream areas. Utilizing this approach, an initial comprehensive climatological analysis of
458 foehn events in Beijing was conducted, revealing that the annual average number of foehn days in the
459 region is 56.5, with notable differences in mean and maximum foehn days across years, exhibiting
460 fluctuating trends over time. Seasonally, foehn events occur most frequently in winter, followed by spring
461 and autumn and then, finally, summer. Spatial distribution patterns of foehn days show a consistent band-
462 like high-value zone extending from northwest to southeast, with low-value zones primarily in
463 northeastern plains of Beijing, though these patterns vary across seasons. The spatial extent of the
464 foehn influence was more pronounced in 2015 and 2016 compared to other years in the study period.
465 Seasonally, the foehn influence reached its maximum extent in the spring and was most limited
466 during summer months. Foehn-induced maximum hourly temperature increases can exceed 11 °C, with
467 peak warming typically occurring from nighttime to early morning, while the minimum temperature
468 changes are generally observed from noon to pre-sunset. Monthly analysis reveals that stations near
469 mountains experience the largest fluctuations in temperature increases, whereas plain stations farthest
470 from the mountains show the smallest variations. The average magnitude of the temperature
471 increase across all stations typically reaches its minimum in July, with a comparatively smaller range of
472 fluctuations relative to other months. Conversely, the maximum temperature increases generally occur in
473 autumn. The most substantial foehn-induced hourly temperature rises are often observed in February.

474 Foehn winds in Beijing have intimate ties with air-pollution episodes, with approximately 67% of
475 pollution episodes accompanied by a foehn. There exists a negative correlation between foehn duration
476 and pollution episode length, where longer pollution episodes encompass a smaller proportion of foehn
477 periods. During pollution events, foehn events predominantly coincide with declining PM_{2.5}
478 concentrations; among pollution episodes featuring foehn winds, 60.4% see a decrease in PM_{2.5}, while
479 39.6% observe an increase. The relationship between the maximum temperature rise during foehn events
480 and changes in PM_{2.5} concentrations is weakly negative. Instances of PM_{2.5} concentrations surging
481 over 50 µg m⁻³ primarily coincide with weak foehn events characterized by temperature increases below
482 2 °C. Foehn events influence pollution episodes through two primary mechanisms: a direct
483 mechanism causing rapid pollutant decrease, and an indirect mechanism characterized by a slight initial
484 decrease followed by a rapid increase in pollutant concentrations. The former typically involves a strong
485 pressure gradient perpendicular to the Taihang Mountains, linked with cold air outbreaks, enabling
486 efficient pollutant clearance due to stronger foehn winds; the latter occurs in milder meteorological
487 settings, with weak foehn winds only marginally lowering pollution levels, insufficient for clearance, and
488 subsequently, alterations to local flow fields and boundary-layer structures by foehn winds lead to rapid
489 pollutant accumulation and increases.

490 The foehn identification method proposed in this study, which relies solely on surface AWS data,
491 facilitates the identification of foehn events using long-term historical observational data. This approach
492 enhances researchers' ability to investigate the relationships and interactions between foehn winds
493 and high-impact weather phenomena.



494 *Data availability.* The PM_{2.5} data are available on the website <https://quotsoft.net/air/>. Other data can
495 be requested from the corresponding author (jli@ium.cn).

496

497 *Author contributions.* JL had the original idea; JL, ZJ, BM, JS, QL, and XJ performed the
498 integrative data analysis; JL and MB wrote the manuscript. All authors discussed the results and
499 commented on the paper.

500

501 *Competing interests.* The authors declare that they have no conflict of interest.

502

503 *Acknowledgments.* The authors would like to thank the anonymous reviewers for their helpful
504 comments. This work was supported by the Beijing Natural Science Foundation (8222048),
505 National Key R&D Program of China (2023YFC3007805), and the Open Grants of the State Key
506 Laboratory of Severe Weather (2022LASW-A03).

507



508 **References**

- 509 Barry, R. G.: Mountain Weather and Climate. 3rd ed. Cambridge University Press, 506 pp, 2008.
510 Brinkmann, W. A. R.: What is a foehn? Weather, 26, 230–240, 1971.
511 Brinkmann, W.A.R.: Strong downslope winds at Boulder, Colorado. Monthly Weather Review,
512 102(8), 592–602. [https://doi.org/10.1175/1520-0493\(1974\)102<0592:SDWABC>2.0.CO;2](https://doi.org/10.1175/1520-0493(1974)102<0592:SDWABC>2.0.CO;2),
513 1974.
514 Cetti, C., Buzzi, M. and Sprenger, M.: Climatology of alpine north foehn. Scientific Reports, 100,
515 76, 2015.
516 Cook, A. J., A. J. Fox, D. G. Vaughan, and J. G. Ferrigno: Retreating glacier fronts on the Antarctic
517 Peninsula over the past half-century. Science, 308, 541–544, doi:10.1126/science.1104235, 2005.
518 Drobinski, P.R., et al.: Foehn in the Rhine valley during MAP: A review of its multiscale dynamics
519 in complex valley geometry. Quarterly Journal of the Royal Meteorological Society, 133(625),
520 897–916. <https://doi.org/10.1002/qj.70>, 2007.
521 Durran, D.R.: Another look at downslope windstorms. Part I: the development of analogs to
522 supercritical flow in an infinitely deep, continuously stratified fluid. Journal of the Atmospheric
523 Sciences, 43(21), 2527–2543. [https://doi.org/10.1175/1520-0469\(1986\)043<2527:ALADWP>2.0.CO;2](https://doi.org/10.1175/1520-0469(1986)043<2527:ALADWP>2.0.CO;2), 1986.
524 Elvidge, A.D., Munneke, P.K., King, J.C., Renfrew, I.A. and Gilbert, E.: Atmospheric drivers of
525 melt on Larsen C ice shelf: surface energy budget regimes and the impact of foehn. Journal of
526 Geophysical Research. Atmospheres, 125(17), e2020JD032463.
527 <https://doi.org/10.1029/2020JD032463>, 2020.
528 Elvidge, A.D., Renfrew, I.A., King, J.C., Orr, A. and Lachlan-Cope, T.A.: Foehn warming
529 distributions in non-linear and linear flow regimes: A focus on the Antarctic Peninsula. Quarterly
530 Journal of the Royal Meteorological Society, 142(695), 618–631. <https://doi.org/10.1002/qj.2489>,
531 2016.
532 Gohm, A. and Mayr, G.J.: Hydraulic aspects of föhn winds in an alpine valley. Quarterly Journal of
533 the Royal Meteorological Society, 130(597), 449–480. <https://doi.org/10.1256/qj.03.28>, 2004.
534 Guzman-Morales, J., Gershunov, A., Theiss, J., Li, H. and Cayan, D.: Santa Ana winds of Southern
535 California: their climatology, extremes, and behavior spanning six and a half decades.
536 Geophysical Research Letters, 43(6), 2827–2834. <https://doi.org/10.1002/2016GL067887>, 2016.
537 Haid, M., Gohm, A., Umek, L., Ward, H.C., Muschinski, T., Lehner, L. and Rotach, M.W.: Foehn-
538 cold pool interactions in the Inn Valley during PIANO IOP2. Quarterly Journal of the Royal
539 Meteorological Society, 146(728), 1232–1263. <https://doi.org/10.1002/qj.3735>, 2020.
540 Hoinka, K.P.: Observation of the airflow over the alps during a foehn event. Quarterly Journal of
541 the Royal Meteorological Society, 111, 199–224, 1985b.
542 Hoinka, K.P.: What is a foehn clearance? Bulletin of the American Meteorological Society, 66(9),
543 1123–1132. [https://doi.org/10.1175/1520-0477\(1985\)066<1123:WIAFC>2.0.CO;2](https://doi.org/10.1175/1520-0477(1985)066<1123:WIAFC>2.0.CO;2), 1985a.
544 Jansing, L., Papritz, L., Dürr, B., Gerstgrasser, D., and Sprenger, M.: Classification of Alpine south
545 foehn based on 5 years of kilometre-scale analysis data, Weather Clim. Dynam., 3, 1113–1138,
546 <https://doi.org/10.5194/wcd-3-1113-2022>, 2022.
547 Jaubert, G., Bougeault, P., Berger, H., Chimani, B., Flamant, C., Häberli, C., Lothon, M., Nuret, M.
548 and Vogt, S.: Numerical simulation of meso-gamma scale features of föhn at ground level in the
549 Rhine valley. Quarterly Journal of the Royal Meteorological Society, 131(608), 1339–1361.
550



- 551 <https://doi.org/10.1256/qj.03.197>, 2005.
- 552 Kohonen, T.: Self-organizing Maps. Springer-Verlag, Heidelberg, 1995.
- 553 Kuipers Munneke, P., M. R. van den Broeke, J. C. King, T. Gray, and C. H. Reijmer: Near-surface
554 climate and surface energy budget of Larsen C Ice Shelf, Antarctic Peninsula. *Cryosphere*, 6,
555 353–363, doi:10.5194/tc-6-353-2012, 2012.
- 556 Kusaka, H. and Fudeyasu, H.: Review of downslope windstorms in Japan. *Wind and Structures*,
557 24(6), 637–656. <https://doi.org/10.12989/was.2017.24.6.637>, 2017.
- 558 Kusaka, H., Nishi, A., Kakinuma, A., Doan, Q. V., Onodera, T., & Endo, S.: Japan's south foehn on
559 the Toyama Plain: Dynamical or thermodynamical mechanisms?. *International Journal of*
560 *Climatology*, 41(11), 5350-5367, 2021.
- 561 Li, Ju, Sun, Zhaobin., et al: A foehn-induced haze front in Beijing: observations and implications.
562 *Atmos. Chem. Phys.*, 20(24), 15793–15809, <https://doi.org/10.5194/acp-20-15793-2020>, 2020.
- 563 Li, X., Xia, X., Wang, L., Cai, R., Zhao, L., Feng, Z., Ren, Q., and Zhao, K.: The role of foehn in
564 the formation of heavy air pollution events in Urumqi, China. *J. Geophys. Res.-Atmos.*, 120,
565 5371–5384, <https://doi.org/10.1002/2014jd022778>, 2015.
- 566 Lian, Z. L., Gao, L. S., Zhao, Y. C., Kuang, S. S.: Climate Characteristic and Formation Mechanism
567 of Continuing High Temperature of Summer in Shijiazhuang, *Chinese Journal of*
568 *Agrometeorology*, 29(4):387-391, 2008 (in Chinese).
- 569 Liao Zhiheng, Xie Jielan, Fang Xingqin, Wang Yu, Zhang Yu, Xu Xinqi, Fan Shaojia, Modulation
570 of synoptic circulation to dry season PM2.5 pollution over the Pearl River Delta region: An
571 investigation based on self-organizing maps, *Atmospheric Environment*, Volume 230, 117482,
572 2020.
- 573 Liu, S., Liu, Z., Li, J., Wang, Y., Ma, Y., Sheng, L., Liu, H., Liang, F., Xin, G., and Wang, J.:
574 Numerical simulation for the coupling effect of local atmospheric circulations over the area of
575 Beijing, Tianjin and Hebei province, *Sci. China Ser. D*, 52, 382–392,
576 <https://doi.org/10.1007/s11430-009-0030-2>, 2009.
- 577 Ma, Q., Wu, Y., Zhang, D., Wang, X., Xia, Y., Liu, X., Tian, P., Han, Z., Xia, X., Wang, Y., and Zhang,
578 R.: Roles of regional transport and heterogeneous reactions in the PM2.5 increase during winter
579 haze episodes in Beijing, *Sci. Total Environ.*, 599–600, 246–253,
580 <https://doi.org/10.1016/j.scitotenv.2017.04.193>, 2017.
- 581 McGowan, H.A. and Sturman, A.P.: Regional and local scale characteristics of foehn wind events
582 over the South Island of New Zealand. *Meteorology and Atmospheric Physics*, 58, 151–164.
583 <https://doi.org/10.1007/BF01027562>, 1996.
- 584 McGowan, H.A., Sturman, A.P., Kossmann, M. and Zawar-Reza, P.: Observations of foehn onset in
585 the southern Alps, New Zealand. *Meteorology and Atmospheric Physics*, 79, 215–230.
586 <https://doi.org/10.1007/s007030200004>, 2002.
- 587 Miltenberger, A.K., Reynolds, S. and Sprenger, M.: Revisiting the latent heating contribution to
588 foehn warming: Lagrangian analysis of two foehn events over the Swiss Alps. *Quarterly Journal*
589 *of the Royal Meteorological Society*, 142(698), 2194–2204. <https://doi.org/10.1002/qj.2816>,
590 2016.
- 591 Nishi, A. and Kusaka, H.: Effect of foehn wind on record-breaking high temperature event (41.1
592 degrees C) at Kumagaya on 23 July 2018. *SOLA*, 15, 17–21. <https://doi.org/10.2151/sola.2019-004>, 2019.
- 593
594 Nishi, A., Kusaka, H., Vitanova, L.L. and Imai, Y. : Contributions of foehn and urban heat Island to



- 595 the extreme high-temperature event in Niigata city during the night of 23–24 August 2018. SOLA,
596 15, 132–136. <https://doi.org/10.2151/sola.2019-024>, 2019.
- 597 Ohba, M. and Sugimoto, S.: Impacts of climate change on heavy wet snowfall in Japan. *Climate*
598 *Dynamics*, 54, 3151–3164. <https://doi.org/10.1007/s00382-020-05163-z>, 2020.
- 599 Ólafsson, H.: The heat source of the foehn. *Hrvat. Meteor. Časopis*, 40, 542–545, 2005.
- 600 Orr, A., Marshall, G.J., Hunt, J.C., Sommeria, J., Wang, C.G., Van Lipzig, N.P., Cresswell, D. and
601 King, J.C.: Characteristics of summer airflow over the Antarctic Peninsula in response to recent
602 strengthening of westerly circumpolar winds. *Journal of the Atmospheric Sciences*, 65(4), 1396–
603 1413. <https://doi.org/10.1175/2007JAS2498.1>, 2008.
- 604 Raphael, M.N.: The Santa Ana winds of California. *Earth Interactions*, 7(8), 1–13.
605 [https://doi.org/10.1175/1087-3562\(2003\)007<0001:TSAWOC>2.0.CO;2](https://doi.org/10.1175/1087-3562(2003)007<0001:TSAWOC>2.0.CO;2), 2003.
- 606 Richner, H., and P. Hächler: Understanding and forecasting Alpine foehn. *Mountain Weather*
607 *Research and Forecasting: Recent Progress and Current Challenges*, F. K. Chow, S. F. J. De
608 Wekker, and B. J. Snyder, Eds., Springer, 219–260, 2013.
- 609 Rolinski, T., Capps, S.B. and Zhuang, W.: Santa Ana winds: A descriptive climatology. *Weather and*
610 *Forecasting*, 34(2), 257–275. <https://doi.org/10.1175/WAF-D-18-0160.1>, 2019.
- 611 Seibert, P., H. Feldmann, B. Neining, M. B?umle, and T. Trickl: South foehn and ozone in the
612 eastern Alps—Case study and climatological aspects. *Atmos. Environ.*, 34, 1379–1394,
613 doi:10.1016/S1352-2310(99)00439-2, 2000.
- 614 Seibert, P.: South foehn studies since the ALPEX experiment. *Meteorology and Atmospheric*
615 *Physics*, 43, 91–103. <https://doi.org/10.1007/BF01028112>, 1990.
- 616 Sharples, J. J., G. A. Mills, R. H. D. McRae, and R. O. Weber: Foehn-like winds and elevated fire
617 danger conditions in southeastern Australia. *J. Appl. Meteor. Climatol.*, 49, 1067–1095,
618 doi:10.1175/2010JAMC2219.1, 2010.
- 619 Shibata, Y., Kawamura, R. and Hatsushika, H.: Role of large-scale circulation in triggering foehns
620 in the Hokuriku district of Japan during midsummer. *Journal of the Meteorological Society of*
621 *Japan*, 88(3), 313–324. <https://doi.org/10.2151/jmsj.2010-304>, 2010.
- 622 Speirs, J.C., McGowan, H.A., Steinhoff, D.F. and Bromwich, D.H.: Regional climate variability
623 driven by foehn winds in the McMurdo Dry Valleys, Antarctica. *Int. J. Climatol.*, 33: 945–
624 958. <https://doi.org/10.1002/joc.3481>, 2013.
- 625 Sun, Y., Chen, C., Zhang, Y., Xu, W., Zhou, L., Cheng, X., Zheng, H., Ji, D., Li, J., Tang, X., Fu, P.,
626 and Wang, Z.: Rapid formation and evolution of an extreme haze episode in Northern China
627 during winter 2015, *Sci. Rep.-UK*, 6, 27151, <https://doi.org/10.1038/srep27151>, 2016.
- 628 Taihang Mountains Based on Background Method, *Meteorological Science and Technology*,
629 48(3):433–437, 2020 (in Chinese).
- 630 Takane, Y. and Kusaka, H.: Formation mechanisms of the extreme high surface air temperature of
631 40.9°C, observed in the Tokyo metropolitan area: considerations of dynamic foehn and foehn like
632 wind. *Journal of Applied Meteorology and Climatology*, 50(9), 1827–1841.
633 <https://doi.org/10.1175/JAMC-D-10-05032.1>, 2011.
- 634 Turton, J.V., Kirchaessner, A., Ross, A.N. and King, J.C.: The spatial distribution and temporal
635 variability of föhn winds over the Larsen C ice shelf, Antarctica. *Quarterly Journal of the Royal*
636 *Meteorological Society*, 144(713), 1169–1178. <https://doi.org/10.1002/qj.3284>, 2018.
- 637 Walker, A. and Ruffner, H.: Föhnforschung und Traubenreife, *Schweiz. Z. Obst-Weinbau*, 9, 245–
638 247, 1998.



- 639 Wang, Xiaoyan & Zhang, Renhe. (2020). Effects of atmospheric circulations on the interannual
640 variation in PM_{2.5} concentrations over the Beijing–Tianjin–Hebei region in 2013–
641 2018. *Atmospheric Chemistry and Physics*. 20. 7667–7682. 10.5194/acp-20-7667-2020.
- 642 Wang, Y., Bao, S., Wang, S., Hu, Y., Shi, X., Wang, J., Zhao, B., Jiang, J., Zheng, M., Wu, M., Ruseel,
643 A., Wang, Y., and Hao, J.: Local and regional contributions to fine particulate matter in Beijing
644 during heavy haze episodes, *Sci. Total Environ.*, 580, 283–296,
645 <https://doi.org/10.1016/j.scitotenv.2016.12.127>, 2017.
- 646 Wang, Z. M., Ding, Y. H., Zhang, Y. X., Fan, J. H., Zhang, S. B., Tian, L. Q.: Feature and Mechanism
647 of the Foehn Weather on East Slope Taihang Mountains II: Case Analysis of the Effects of Lee
648 Wave on Foehn Occurring and Moving, *Plateau Meteorology*, 31(2): 555–561, 2012b (in Chinese).
- 649 Wang, Z. M., Ding, Y. H., Zhang, Y. X., Wang, C. M., Li, J. B., Gu, Y. L.: Feature and Mechanism
650 of the Foehn Weather on East Slope Taihang Mountains I: Statistic Feature, *Plateau Meteorology*,
651 31(2):547–554, 2012a (in Chinese).
- 652 Westerling, A. L., D. R. Cayan, T. J. Brown, B. L. Hall, and L. G. Riddle: Climate, Santa Ana winds
653 and autumn wildfires in southern California. *Eos, Trans. Amer. Geophys. Union*, 85, 289–296,
654 doi:10.1029/2004EO310001, 2004.
- 655 Whiteman, C. D.: *Mountain Meteorology: Fundamentals and Applications*, Oxford Univ. Press,
656 New York, 2000.
- 657 WMO: *International Meteorological Vocabulary*, WMO No.182, 1992.
- 658 Würsch, M. and Sprenger, M.: Swiss and Austrian Foehn revisited: A Lagrangian-based analysis.
659 *Meteorologische Zeitschrift*, 24(3), 225–242. <https://doi.org/10.1127/metz/2015/0647>, 2015.
- 660 Xiong, X. P., Wang, S. Y., Zhang, W.: Analysis of Foehn Characteristics in Middle Section of
661 Taihang Mountains Based on Background Method, *Meteorological Science and Technology*,
662 48(3):433–437, 2020 (in Chinese).
- 663 Yang, X. L., Yang, M., Li, J. B., Zhang, S.: Impact Analysis of a Taihang Mountain Fohn on Haze
664 Intensity, *Meteorological Monthly*, 44(2):313–319, 2018 (in Chinese).
- 665 Zhao, B., Wang, P., Ma, J. Z., Zhu, S., Pozzer, A., and Li, W.: A high-resolution emission inventory
666 of primary pollutants for the Huabei region, China, *Atmos. Chem. Phys.*, 12, 481–501,
667 <https://doi.org/10.5194/acp-12-481-2012>, 2012.
- 668 Zhao, S. X., Wang, R. K., Guo, Y. B., Tan, J. L., Shi, Z. Z.: The Foehn in the Middle Range of
669 Taihang Mountain, *Meteorological Monthly*, 19(2):3–6, 1993 (in Chinese).
- 670 Zhang, J. J. and Li, J.: A Study on the Identification of Foehn Winds Using Automatic
671 Meteorological Station Data in Conjunction with GNSS Data, *Meteorological Monthly*,
672 submitted, 1993 (in Chinese).
- 673 Zheng, G. J., Duan, F. K., Su, H., Ma, Y. L., Cheng, Y., Zheng, B., Zhang, Q., Huang, T., Kimoto,
674 T., Chang, D., Pöschl, U., Cheng, Y. F., and He, K. B.: Exploring the severe winter haze in Beijing:
675 the impact of synoptic weather, regional transport and heterogeneous reactions, *Atmos. Chem.*
676 *Phys.*, 15, 2969–2983, <https://doi.org/10.5194/acp-15-2969-2015>, 2015.
- 677